

# TEXasGAN: Tactile Texture Exploration and Synthesis System Using Generative Adversarial Network

Mingxin Zhang, Shun Terui, Yasutoshi Makino, Hiroyuki Shinoda

**Abstract**—To create more realistic experiences in human-virtual object interactions, texture rendering has become a research hotspot in recent years. Different frequency components of designed vibrations can activate texture-related sensations due to similar receptors. However, designing specific vibrations for numerous real-world materials is impractical. Therefore, this study proposes a human-in-the-loop vibration generation model based on user preferences. To enable users to easily control the generation of vibration samples with large parameter spaces, we introduce an optimization model based on Differential Subspace Search (DSS) and Generative Adversarial Network (GAN). With DSS, users can use a one-dimensional slider to easily modify the high-dimensional latent space so that the GAN can generate desired vibrations. We trained the generative model using an open dataset of tactile vibration data and selected five types of vibrations as target samples for the generation experiment. Extensive user experiments were conducted using the generated and real samples. The results indicate that our system can generate distinguishable samples that match the target characteristics. Moreover, the results also reveal a correlation between subjects' ability to distinguish real samples and their ability to distinguish generated samples.

**Index Terms**—Haptic display, Human-computer interaction, Optimization, Deep learning, Autoencoder, Generative adversarial networks

## I. INTRODUCTION

Nowadays, the virtual realm built by information technologies has become an integral part of daily life. Among various interaction technologies, haptics, which enables natural and intuitive tactile interaction with virtual objects and surfaces, can make users to engage with this information-rich virtual world and improve the user experience [1], [2]. In the research field of haptics, the rendering of texture of objects has been a hot and an active topic to augment the user experience in Virtual Reality (VR) or other application scenarios [3], [4], [5]. We can make the users feel the sensation of some certain objects or textures using vibration stimuli. Nonetheless, the precise replication of tactile textures that closely approximate real-world surfaces remains a formidable undertaking.

One way to present rich tactile information is through vibration stimuli due to related tactile receptors [6]. There are two methods for generating vibration stimuli: recording the

actual vibration using a sensor or microphone and playing it back, or manually designing the vibration waveform. The latter is especially useful when direct measurement is not possible, such as in video games or when enhancing specific tactile sensations for richer feedback. In this study, we focus on generating tactile sensations by tuning parameters in vibrotactile stimuli.

The difficulty in designing such a vibration manually is that there are many parameters to tune [3]. The diversity and abundance of tactile textures in the physical world makes it impractical to create specific models for each texture. Therefore, developing a system that can dynamically accommodate a wide range of vibration patterns while optimizing the associated parameters is highly valuable.

There have been many studies concentrated on the reconstruction of vibration signals through the utilization of spectrograms derived from sensor data capturing physical surface interactions, and also gave the optimized spectrograms that match the desired texture pattern well using generative models [4], [7]. In pursuit of a broader and more versatile spectrogram of vibrotactile signals, deep learning based generative models, particularly Generative Adversarial Network (GAN), have been enlisted. These methods can effectively optimize the objective function and yield satisfactory generative results. Building upon this, we also recognize that human expert knowledge may be another crucial factor influencing the optimization, particularly in tasks related to subjective perception.

The assistance of human knowledge allows us to treat vibration patterns that are similar in terms of human perception, even if they are different in terms of power spectrum images. Consequently, integrating human judgment and sensibility into the optimization process, a concept known as “human-in-the-loop”, becomes an appealing approach to yield results that resonate with human subjective perception, as posited in [7], [8], [9].

However, optimizing vibrotactile signals, which often involves multiple parameters, presents a significant challenge for manual adjustment within the latent space. Techniques like SLS [8] enable users to manipulate multiple parameters through a one-dimensional (1-D) slider. Additionally, other interactive methods have been used to involve humans in the optimization process, such as offering different generation results for users to choose from, thereby influencing the optimization direction and generating novel textures beyond the known training dataset [7]. Considering these complexities,

This work was supported in part by the JST SPRING, Grant Number JPMJSP2108.

Mingxin Zhang, Shun Terui, Yasutoshi Makino, Hiroyuki Shinoda are with the Department of Complexity Science and Engineering, The University of Tokyo, Chiba 277-8561, Japan (e-mail: m.zhang@hapis.k.u-tokyo.ac.jp, terui@hapis.k.u-tokyo.ac.jp, yasutoshi\_makino@k.u-tokyo.ac.jp, hiroyuki\_shinoda@k.u-tokyo.ac.jp).

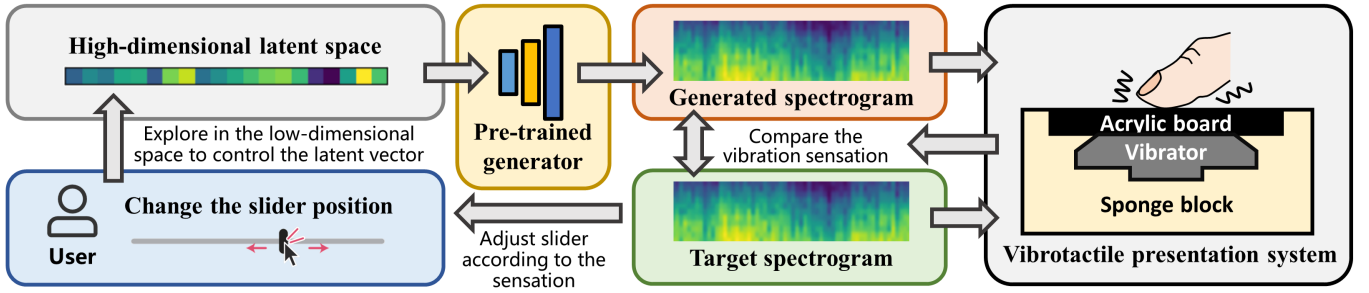


Fig. 1. The structure of our optimization system. Users can easily control the high-dimensional latent vector with a 1-D slider, and the generator can give spectrograms according to the latent vector. Users can compare the tactile sensation of the generated vibration and the real target, and update the optimizer by the slider position corresponding to the closest result to the target.

conventional Bayesian optimization techniques like SLS [9] may face limitations. Our goal is to provide users with a continuous exploration approach within the latent space, ensuring the optimization process is seamless and free from potential discontinuities.

In this paper, we introduce TEXasGAN, a system designed to allow users to create customized vibrotactile feedback based on their subjective perceptions, as shown in Fig. 1. Our approach utilizes the Differential Subspace Search (DSS) method [9], enabling users to explore a high-dimensional latent space through a 1-D slider. To address the challenge of reaching every point in the latent space, we also implemented an initialization method to provide a good starting point. We trained GAN-based neural network models and used the pre-trained generator to create spectrograms from latent vectors optimized via DSS. The user interface features a simple 1-D slider, enabling users to experience and evaluate generated tactile vibrations. Through iterative exploration and selection, users can identify the optimal slider position that yields vibrations closest to their desired stimulus. Our two-stage user experiment, consisting of generation and evaluation phases, demonstrated that TEXasGAN can produce distinguishable vibrations. Despite the extensive research on human-in-the-loop approaches in various interaction methods, their application in haptics remains underexplored. We hope our work contributes to the development of more intuitive and realistic haptic feedback systems.

## II. RELATED WORK

### A. Vibration Tactile Presentation

Significant progress has been achieved in the advancement of vibrotactile haptic devices, making them a central focus of investigation within the domain of tactile presentation systems. Numerous studies have been dedicated to the replication of diverse sensory experiences. For instance, through the utilization of piezo actuators, vibrotactile feedback on touchscreens has been employed to simulate the tactile sensation of physical buttons, as exemplified in the work by Sadia et al. [10]. Beyond touchscreen interactions, wearable devices like FingerX [11] have emerged to offer users a heightened sense of object shapes within VR environments.

Among the array of sensory modalities, the recreation of tactile textures has garnered significant attention. Through the

capture of sound recordings while traversing real surfaces, the corresponding texture-specific vibrations can be faithfully reproduced via audio signals [12]. Nevertheless, it is noteworthy that this research underscores the necessity of meeting specific requirements in terms of both time resolution and frequency resolution to effectively replicate tactile sensations. Furthermore, it highlights the critical role of parameter design in shaping the characteristics of the vibrotactile signal.

### B. Generative Neural Network

In addressing parameter design challenges in the domain of vibrotactile texture reproduction, a variety of optimization algorithms have been applied, as highlighted in recent works [13], [14], [15]. However, for scenarios involving a substantial number of parameters, deep learning techniques, which have seen significant advancements in recent years, have emerged as a more effective solution for managing the intricate optimization aspects of texture generation.

Autoencoders, owing to their relatively straightforward architecture and unsupervised training paradigm, have been employed in some studies to serve as tools for compressing and reconstructing tactile signals [16], [17]. Nevertheless, the compression process can introduce oversmoothing, resulting in the loss of fine-grained details, making autoencoders difficult to reproduce detailed texture related vibration signals. Although increasing the dimension of the compressed latent vector can solve the problem, it also makes operations like optimization more difficult. Therefore, the use of generative models, rather than a decoder within the autoencoder framework, to reconstruct vibration signals has become a prudent choice.

GAN, a prominent generative neural network model, has garnered widespread recognition for its applications in image generation and is progressively finding utility in diverse tactile reconstruction tasks as well [7], [4], [18]. GAN primarily comprises two components: the generator and the discriminator. The generator is tasked with generating samples from a specified distribution, commonly Gaussian noise, while the discriminator's role is to differentiate between samples generated by the generator and real samples. Through an iterative training process, the discriminator's proficiency in discerning genuine from generated samples continually improves. Simul-

taneously, guided by the discriminator, the generator becomes increasingly good at producing more real samples.

The remarkable generative capabilities of GAN enable it not only to generate samples from random noise but also from specific distributions, affording controlled sample generation opportunities. For example, prior research has explored the generation of surface images from vibrations [19] and, conversely, the generation of vibration signals from texture images [4], [18]. This characteristic of GAN, which encompasses not just reconstruction but also the generation of “new” samples conforming to a particular distribution while introducing variations, positions GAN as particularly well-suited for optimization problems in which we seek optimal solutions through continuous exploration of the latent space.

### C. Human-in-the-loop Optimization

While GANs excel at generating samples that mathematically resemble real data, in some human evaluation tasks they do not inherently account for subjective cognition. In other words, does a small loss value equate to a similar perception or cognition? Consequently, many studies focused on optimization models incorporating a human-in-the-loop mode, which integrates human involvement into the iterative optimization process. This approach utilizes human expertise to guide the optimization direction.

Some human-in-the-loop systems focus solely on direct parameter optimization [20] of several parameter dimension, while other researches have explored optimization algorithms like Bayesian optimization [8], [21] to enable simultaneous control of multiple parameters. Furthermore, to overcome challenges when dealing with relatively large latent spaces, there have been some studies applying deep learning models in the optimization process to increase the capability of parameter dimension [7], [9]. Another significant challenge in the optimization of deep learning models arises from the difficulty of incorporating human decision-making throughout a large number of training epochs [7].

A previous research offers users the choice to select the optimal texture for optimizing the latent vector instead of optimizing the neural network itself [7]. This approach provides an effective solution for optimizing deep learning models. In our own research, we adopted a similar strategy, employing pre-trained deep learning models and seeking positions in the latent space that correspond to optimal outputs. Furthermore, we employed continuous exploration of the latent space through sliders rather than discrete user interaction methods, facilitating a seamless and comprehensive exploration process.

## III. METHODS

In this section, we will introduce the design and the implementation of our tactile vibration generation system. The whole human-in-the-loop optimization process is shown in Fig. 1. Users can change the vibration and obtain the closest result to the target by changing the slider position. First we will introduce the framework of the optimization method and then we will introduce the design, structure and training of our generative model (as shown in Fig. 2).

### A. Human-in-the-loop Differential Subspace Search

To enable individuals to effectively leverage their knowledge for optimization purposes, it is imperative to ensure that users possess the ability to freely manipulate the resultant oscillatory patterns during each iteration of the optimization loop. However, exerting precise control over a multitude of parameters within a high-dimensional latent space is an intricate challenge.

An efficacious solution to this quandary is presented by the DSS [9]. DSS facilitates optimization in a manner that permits users to maintain command over the high-dimensional latent space while concurrently exploring a relatively lower-dimensional latent space. This approach streamlines the manipulation process for human users, rendering it more manageable and accessible.

The optimization problem can be represented as

$$\mathbf{z}^* = \underset{\mathbf{z} \in \mathcal{Z}}{\operatorname{argmax}} E(G(\mathbf{z})). \quad (1)$$

Here, the generator function  $G$  takes an input latent vector  $\mathbf{z}$  from the high-dimensional latent space  $\mathcal{Z}$ , and the evaluation function  $E$  quantifies the quality of the generated output. In our specific context, the choice of the function  $E$  is contingent upon the subjective perception of the user. The objective of the optimization is to discover the optimal latent vector  $\mathbf{z}^*$  that maximizes the value of the evaluation function  $E$  through human-guided exploration within the latent space [9].

Consequently, the iterative update in the optimization process can be expressed as

$$\mathbf{z}^{(k+1)} = \mathbf{z}^{(k)} + \alpha \left( \frac{\partial E(\mathbf{z}^{(k)})}{\partial \mathbf{z}} \right)^T. \quad (2)$$

The step size  $\alpha$  is chosen to be greater than zero to ensure maximization of the value of the evaluation function.

To simplify user control over the latent vector, DSS introduces an operator denoted as  $p_{\mathbf{z}^{(k)}}(w)$ . This operator transforms a low-dimensional latent vector, specifically a single number  $w$  that represents the slider position within the 1-D space  $W$ , into the corresponding position  $\mathbf{z}^{(k)}$  within the original high-dimensional latent space  $\mathcal{Z}$ . This approach allows users to manipulate only the low-dimensional subspace. Consequently, Eq. 2 can be modified as follows:

$$\mathbf{z}^{(k+1)} = \mathbf{z}^{(k)} + p_{\mathbf{z}^{(k)}}(w). \quad (3)$$

To derive the operator  $p_{\mathbf{z}^{(k)}}(w)$ , the determination of the subspace  $W$  can be accomplished through singular value decomposition (SVD) applied to the Jacobian matrix of the generator [9].

### B. Generator Design

We designed our vibrotactile generator architecture based on the framework of the super-resolution residual network (SR-ResNet) [22], [23]. Our motivation was to effectively address high-frequency image details. There is an input convolutional layer, 16 residual blocks, a mid convolutional layer, a 4-times upscale module consisting of two convolutional layers and two pixel shuffle layer, and an output convolutional layer in the SRResNet. We introduced a Fully Connected (FC) layer to

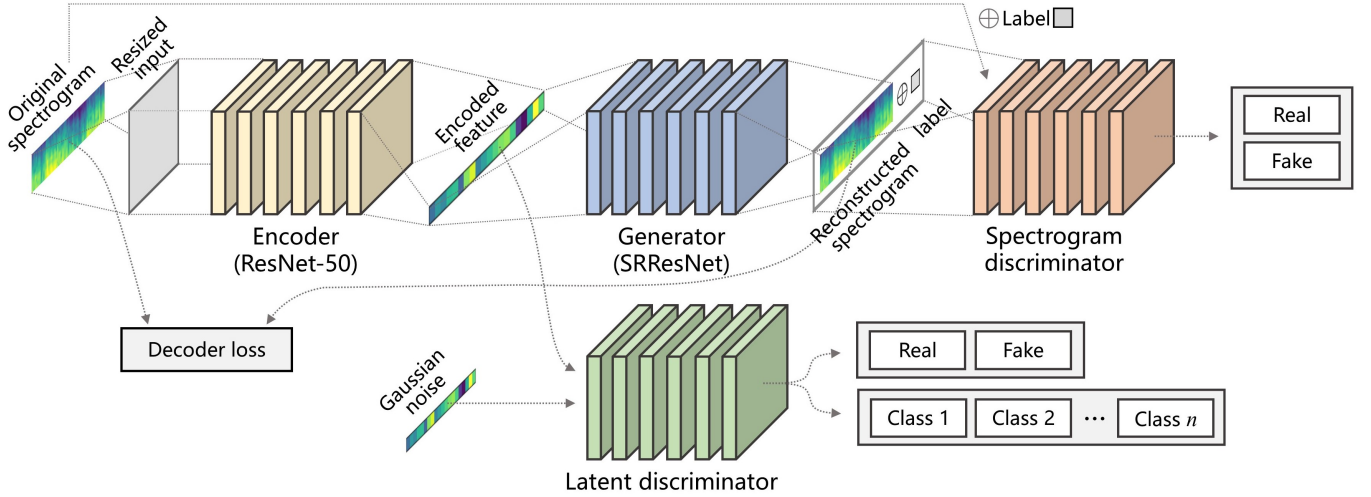


Fig. 2. The structure of the GAN model in this research. The model can generate vibrotactile spectrograms from the latent space built by the ResNet-50 encoder.

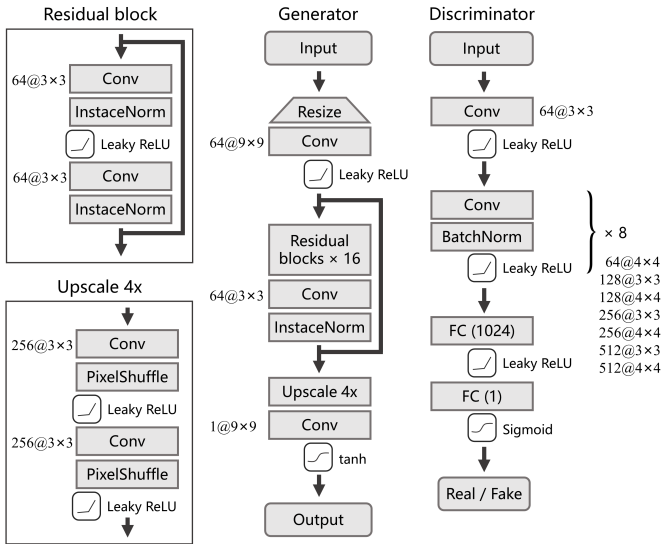


Fig. 3. The structure of the SRResNet-based GAN.

the input end of the network as the resize layer for dimension transformation, so that our latent vector can be received by SRResNet. Additionally, we made an adjustment to the final convolutional layer of the network to tailor the output to the required size, specifically to generate the desired spectrogram.

To ensure the effectiveness of the generator, it is essential to employ an appropriate discriminator. A discriminator that performs exceptionally well or very poorly can hinder the training of the generator. In our study, we utilized a discriminator with a structure akin to the one presented in [22]. This discriminator comprises 8 convolutional layers, albeit with adjustments to the channel numbers to align it with the specific requirements of our task. The comprehensive architecture of the Generative Adversarial Network (GAN) is depicted in Fig. 3.

The generator and the discriminator was trained simultaneously, and in the training process, the generator  $G$  will learn how to generate new samples closer to the real sample, while

the discriminator  $D$  will discriminate the generated samples. The goal of the training can be represented as follows:

$$\min_G \max_D \mathbb{E}_{x \sim p_{data}(x)} [\log(D(x))] + \mathbb{E}_{z \sim p(z)} [\log(1 - D(G(z)))] \quad (4)$$

where  $z$  means a random noise from the distribution  $p(z)$  (Gaussian distribution in this research), and the  $p_{data}(x)$  denotes the distribution of the real data  $x$ . This competitive process encourages the generator to generate samples that are indistinguishable from real data.

### C. Generation with Conditional Knowledge

While GAN has outstanding generation performance, the training process is not very stable. Additionally, GAN generate samples from random noise, resulting in uncontrollable outcomes. However, our objective is to exert control over the latent space, enabling the model to generate spectrograms that closely resemble real samples belonging to specific classes. To address these challenges, we built our model combining the advantages of GANs and autoencoders, and utilized conditional information. The inspiration for our model draws from previous works such as Auxiliary Classifier GAN (ACGAN) [24], Autoencoding GAN (AEGAN) [25], and Conditional Adversarial Autoencoder (CAAE) [26] to enhance the training process and enable the model to generate samples belonging to given classes.

Our model shown in Fig. 2 contains four parts: encoder, generator, spectrogram discriminator, and latent discriminator. The encoder extracts the feature vector from the original spectrogram, while the generator utilizes this feature vector to reconstruct the spectrogram. Similar to the Adversarial Autoencoder (AAE) paradigm, a latent discriminator is employed to encourage the encoder's output to conform to a predetermined prior distribution. This ensures that the latent space is evenly distributed according to the specified prior distribution, allowing the generator to effectively learn a mapping from this prior distribution to the spectrogram distribution,

as proposed in [27]. Additionally, a determined distribution will also benefit the following optimization of DSS. To make the feature containing richer information, we also utilized the spectrogram discriminator as a classifier and applied the auxiliary classification loss, such as the ACGAN. It will work as the discriminator and classifier when receives the encoded feature, and only as the discriminator when receives the real gaussian noise.

To avoid data loss in compression and over-smoothing reconstruction, we used a generator together with the decoder loss, and use a weight value to balance them. The generator and spectrogram discriminator were structured according to the principles of CAAE. Notably, with the label as the conditional information, the generator can generate samples belonging to certain classes. And the discriminator can learn the relationship in the pairs of the spectrogram and the corresponding class, help the generator to give correct spectrograms. The training goal can be described as follows:

$$\begin{aligned}
 \min_{E,G,C} \max_{D_z,D_s} & \lambda \mathcal{L}(G(E(x), y), x) + \gamma TV(G(E(x), y)) \\
 & + \mathbb{E}_{z \sim p(z)} [\log(D_z(z))] \\
 & + \mathbb{E}_{x,y \sim p_{data}(x,y)} [\log(1 - D_z(E(x)))] \\
 & + \mathbb{E}_{x,y \sim p_{data}(x,y)} \left[ \sum_i y_i \log(C(E(x))) \right] \\
 & + \mathbb{E}_{x,y \sim p_{data}(x,y)} [\log(D_s(x, y))] \\
 & + \mathbb{E}_{x,y \sim p_{data}(x,y)} [\log(1 - D_s(G(E(x)), y))],
 \end{aligned} \tag{5}$$

where  $D_z$  represents the latent discriminator,  $E$  and  $G$  represent the encoder and generator,  $D_s$  represents the spectrogram discriminator, and  $C$  represent the auxiliary latent classifier, respectively.  $x$  and  $y$  represent the real data and the label.  $TV$  represents the total variation loss.  $\lambda$  and  $\gamma$  are the weights for the decoder loss and the total variation loss, which can balance the smoothness and high resolution [26]. In this paper, the weight setting is  $\lambda = 100$  and  $\gamma = 10$ .

We initialized the encoder using a pre-trained ResNet-50 model that was trained on the ImageNet1K\_V2 dataset, and introduced an FC layer to resize the spectrogram to the shape corresponding to the pre-trained model input. The generator and the spectrogram discriminator follow the network structures illustrated in Fig. 3, maintaining consistency with those architectures. The latent discriminator contains 2 FC layers, and 1 output layer for the discrimination and 1 output layer for the classification. To apply the label as conditional information, we used one-hot labels and used an FC layer to resize the label vector to the dimension corresponding to the feature map. And then the label information will be added to the feature map as a channel.

#### IV. EXPERIMENTS

In this section, we will demonstrate the implementation details of the system and our experiment design.

##### A. Data Preparation

In this study, we employed the LMT108 dataset [28], which includes recordings of 108 distinct textures along with

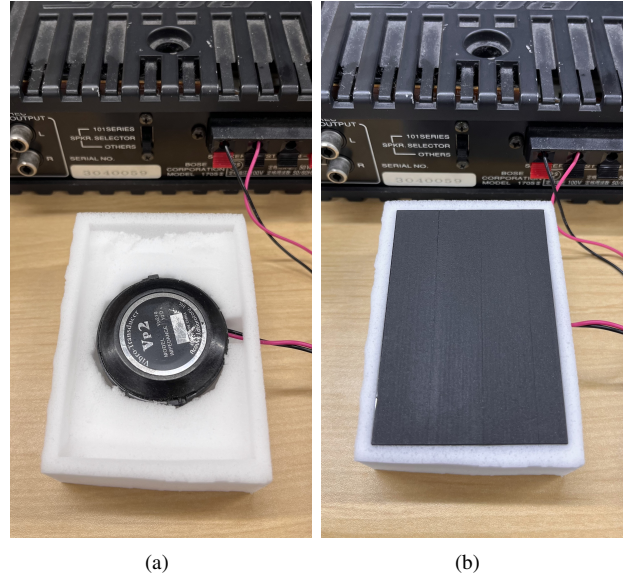


Fig. 4. The vibrotactile presenting device in this research. The vibrator was placed in a sponge block as shown in (a), and a piece of acrylic board was attached to the top of the vibrator for users to touch, as shown in (b).

their corresponding surface images. To construct our training dataset, we utilized the sound recording files capturing the motion of a texture explorer traversing various surfaces.

Seven groups (G1–G4, G6, G8, and G9) were selected from the total of nine groups in LMT108. The G5 and G7 groups were excluded from the study, as the original stimuli were found to evoke a tactile sensation that was similar to that of other groups. And we selected 2 kinds of textures from each group and built a training dataset containing 14 classes.

First, a 3rd-order Butterworth bandpass filter was applied to extract frequency components ranging from 20 Hz to 1000 Hz. Subsequently, the Short Time Fourier Transform (STFT) was employed to construct spectrograms from the audio recordings, with a sampling rate of 44100 Hz. The STFT frame length was configured to 2048, accompanied by a hop length of 0.1 times the frame length. A Hann window was chosen as the windowing function.

To transform spectrograms back into sound waves so that the vibrator can play them, we adopted Griffin-Lim algorithm [29]. The number of samples per frame was set at 2048, the iteration time was set to 50, the hop length was set to 2048 / 10 (floor rounding). To reduce the time cost and provide a smooth interaction experience, we employed the algorithm on GPU using TorchAudio [30].

In order to train the model effectively, we segmented the spectrogram into fragments using a sliding window. This approach yielded several advantages, including dimensionality reduction and an augmentation in the training dataset's size. The dimensions of the sliding window were set at 48 units along the frequency axis and 320 units along the time axis, corresponding to a segmentation of  $48 \times 320$  spectrograms. The choice of 48 on the frequency axis corresponded to 1000 Hz, signifying that only the segment of the spectrogram within this frequency range was retained. Concurrently, the 320 units

along the time axis approximated a duration of 1.5 seconds for each spectrogram segment. This temporal length was deemed sufficient to capture the full information of the underlying audio signal.

The original dataset contains about 5 seconds sound recordings of different surfaces. Here we used a sliding window of  $48 \times 320$  corresponding to about 1.5 seconds, and moved it on transformed spectrograms, so that we can obtain segmentations from different beginning time. The moving step length was set at 5 units (about 23 milliseconds), and produced a total of 24480 spectrogram segments.

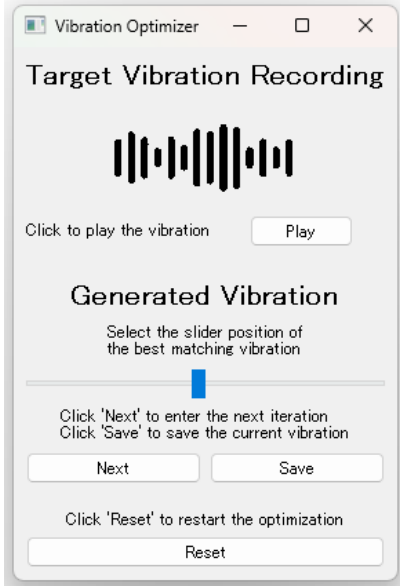


Fig. 5. The user interface of the optimization.

## B. Model Training

The size of the latent vector  $z$  was set to 128. In our attempts, larger latent vector cannot improve the performance obviously, but caused fluctuations and a longer convergence time. Network training hyperparameters were defined as follows: a batch size of 128, the learning rates of  $G$  and  $D_s$  were set to 0.0002, and the  $E$ ,  $C$  and  $D_z$  were set to 0.001. The learning rates of  $C$  and  $D_z$  was decreased by a factor of 0.95 with the increasing of the epoch number. We opted for binary cross-entropy for the adversarial loss and cross-entropy for the auxiliary classification loss, while for the decoder loss, Mean Square Error (MSE) was chosen. The Adam optimizer was employed for efficient optimization. In order to mitigate overfitting, we utilized soft labels within the adversarial component. Specifically, a one-sided label smoothing was implemented, with a soft scale parameter set to 0.3. This signifies that random values between 0.7 and 1 were utilized instead of a fixed value of 1, and similarly, random values between 0 and 0.3 were employed instead of 0. The entire training regimen spanned 50 epochs. After the training process, only the generator part was used the optimization system. The training process was conducted on an RTX A6000 GPU, took 2.5 hours.

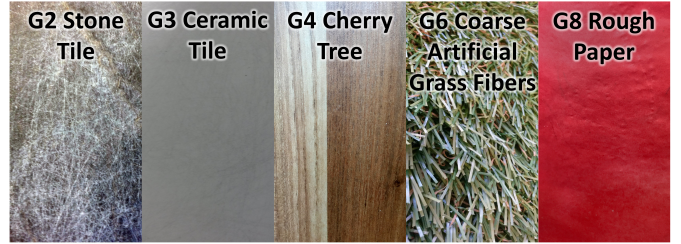


Fig. 6. The selected 5 target classes to generate.

In order to expedite convergence, mitigate bias, and enhance stability, we applied min-max normalization to the training dataset, subsequently rescaling the range of values to fall within the  $[-1, 1]$  range. This normalization process aligns the data range of both the input and output of the generator, facilitating the training process. Additionally, we performed the inverse transformation to revert the network’s output range back to the original real data range, ensuring that the generated data remains consistent with the original data distribution.

## C. Initialization

A better initial point will help the optimizer find the target well. DSS has attempted initialization approaches such as providing options or limiting the distance between initial point and target to control the difficulty of the task and avoid bad initialization [9].

There is a more severe challenge in our optimization setup. While the auxiliary classifier enhances class distinguishability, it widens the gap between classes, potentially hindering the optimizer from traversing between clusters and restricting it to a confined space (details of the latent space distribution in Sec. V-A).

To address this challenge, we used a user option-based initialization method inspired by the tabu search [31], a metaheuristic search technique that incorporates a “prohibition” rule to facilitate solution discovery. Our straightforward initialization rule ensures a quick process.

A vibration of the training set is randomly chosen and transformed into the latent vector  $z$  using the trained encoder, which serves as the initial value. Users compare the initial vibration with the target vibration, selecting a similarity rank from “Good,” “So-so,” or “Bad.” If the user chooses “So-so” or “Bad,” another  $z$  is selected until a “Good” match is identified. The corresponding latent vector  $z'$  is accepted as the initial value for the DSS optimizer.

To bring  $z$  closer to the target area, the principle of our search strategy is: Choose near but different new  $z$  for “So-so”, and far new  $z$  for “Bad”. The average distance of vectors in the latent space  $dis_{avg}$  was calculated. Here we define a parameter  $step = \frac{1}{8} \times dis_{avg}$  as the unit of the moving distance during the exploration. Inspired by the tabu search, visited latent vectors are added to the tabu list. In this study, a specified radius  $r$  is enforced for vectors within the tabu list (here  $r$  is defined as the average distance  $step$ ). Consequently, vectors within this range are prohibited, allowing for the exploration of larger regions. In this study, the length of the tabu list is set to 5, meaning

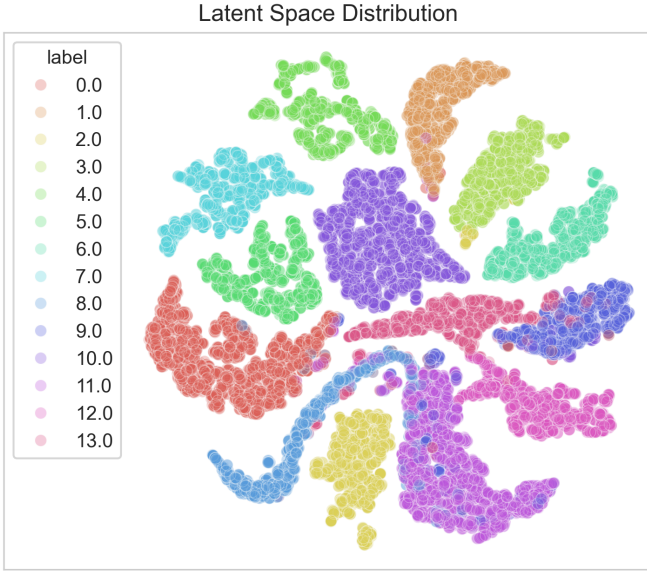


Fig. 7. The distribution visualization of the latent space.

that the areas surrounding the 5 most recently visited latent vectors are prohibited from the further exploration. Following the search principle mentioned, when the user selects “So-so”, we choose a new  $z$  within the range of  $(0.5 \times step, 2 \times step)$  from the current  $z$ . If the user chooses “Bad”, we select a new  $z$  from distances beyond  $2 \times step$  from the current  $z$ .

This simple rule is easy to implement and allows for rapid execution. Through this method, we can efficiently select an initial latent vector that is closer to the target region, mitigating the risk of not being able to reach the target area due to gaps in the distribution of classes.

#### D. User Interface and Presenting Device

Fig. 4 and Fig. 5 show the vibrotactile display for evaluating the designed vibration and the user interface of DSS. The device [12] was composed of a vibro-transducer (Acouve Vp210), a power amplifier (BOSE 1705II), sponge and an acrylic cover board. The vibrator was set in the sponge block so that the vibration can be transmitted effectively. The acrylic board covered with tapes was pasted onto the top surface of the vibrator, so that users can place their fingers on the plane surface and feel the generated vibration.

During the optimization process, users can click the “Play” button above to play the actual vibration recording serving as the target. When users drag the slider below, vibrations generated from the feature vector corresponding to the slider’s position will be played. Users can freely explore the high-dimensional feature space by moving the one-dimensional slider. Once users locate the slider position that best matches the target vibration, they can click “Next” to proceed to the next iteration. Users can also click “Save” at any time to save the currently generated vibration.

#### E. Stage I: Generation

To assess the generative performance of our TEXasGAN, we designed a two-stage experiment that includes a generation experiment and an evaluation experiment. To validate whether TEXasGAN can generate new samples different from the training data, we selected 5 classes from LMT108 that differ from the training set as generation targets, as shown in Fig. 6.

Due to the free movement of the collection device on surfaces during the vibration acquisition process [28], vibration is not uniformly distributed on the time axis. This implies that not all samples can effectively represent the characteristics of a particular class. To provide subjects with more reliable target vibrations, facilitating better execution of the generation task, we manually selected 3 relatively uniform and representative vibrations for each class. This resulted in a total of 15 target vibrations, and subjects were tasked with generating samples as similar as possible to these vibrations.

In comparison to some slider-based human-in-the-loop visual optimization tasks [8], [9], the haptic perception is not as sensitive as vision. To help subjects better understand how to perceive vibration characteristics and the differences between vibrations of different categories, we conducted some training tasks before the main experiment. In this process, we informed subjects about the system’s operation, showed them target vibrations from different classes to help them understand the distinctions, presented target vibrations from the same class to illustrate commonalities, and allowed subjects to perform actual operations to familiarize themselves with the experimental procedure and comprehend our optimization goals.

After subjects familiarized themselves with the system and the characteristics of vibrations, we proceeded to the generation experiment process. Subjects were required to generate a sample corresponding to each target vibration. The first step was the initialization of the optimization process. In this step, subjects needed to use the options “Bad”, “So-so” and “Good” to select a suitable initial value for the optimizer. During this process, subjects were only required to make rough comparisons, so they were instructed not to focus on detailed perceptions, but to perform quick and multiple selections, with the aim of covering as broad an exploration range as possible through multiple attempts. After entering the optimization process, subjects were still encouraged to make as many selections as possible rather than sticking to a single iteration’s slider position selection. However, in this phase, subjects were asked to carefully perceive various aspects of vibrations, such as frequency and amplitude. Moreover, to distinguish between different slider positions, this optimization process might be more time-consuming. When consecutive iterations did not produce vibrations significantly different along the slider direction, subjects could adopt several strategies:

- 1) Continue selecting similar slider positions as much as possible.
- 2) Randomly choose slider positions to help the optimizer move away from the current situation.
- 3) If the subject felt dissatisfied with the current vibration, restart the optimization process.

Following strategy 1 or strategy 2 for several consecutive

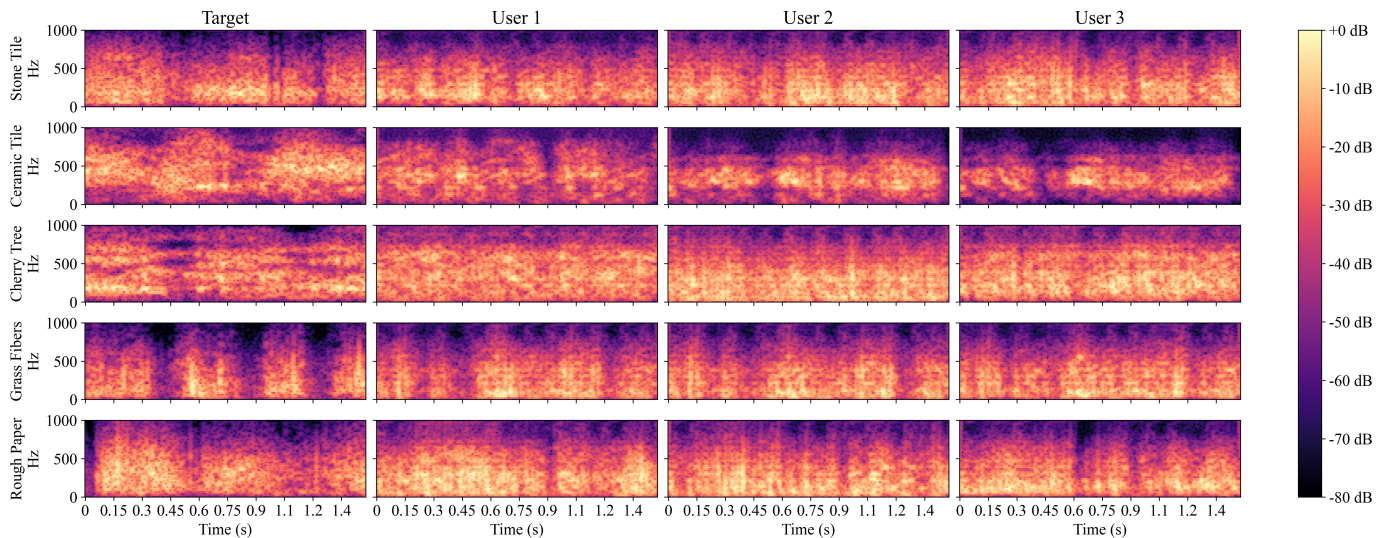


Fig. 8. The figure shows one of the target vibrations for each class, along with the corresponding vibrations generated by 3 users.

iterations usually allowed the optimizer to move away from the current state. During the experiment process, subjects were asked to freely choose strategies based on their subjective judgment. The entire process of the generation experiment lasted approximately 2 hours, including rest breaks. Each subject generated a total of 15 samples corresponding to the target vibrations. From initialization to completion, the generation of each sample took 2-8 minutes.

In order to cover as many generated results as possible in the subsequent pairing task of the evaluation experiment without overwhelming the subjects, we limited the number of generated samples. In the first stage, we invited 3 subjects (3 males, aged 21-26), who totally generated 45 samples (9 for each class). These three subjects will not be involved in the evaluation phase to eliminate the impact of memory.

#### F. Stage II: Evaluation

We designed a classification task to validate the similarity between generated vibrations and real surface vibrations. The classification task comprised three parts:

1. Select the correct class for the real vibration (the control group): In this part, all 15 real vibrations were presented in a shuffled order to the subject. Each time, one vibration was shown, and 5 other randomly selected real vibrations from the 5 classes were also presented (excluding the vibration to be classified). The subject was required to choose the vibration that most closely resembled the presented vibration. This process was repeated three times, resulting in a total of 45 classifications. The aim of this part was to validate the premise of this study, which is that people can perceive differences between vibration stimuli, understand their characteristics, and correctly classify them into corresponding categories. Simultaneously, the conclusions from this control group were used to verify the fidelity of the generated results. We also asked subjects to describe the features of these 5 kinds of vibrations and conduct the following tasks according to these features.

2. Select the correct class for the generated vibration. The procedure of the second part was similar to the first part. However, instead of the real vibration, the vibration to be classified was replaced by the generated vibration. The 45 generated vibrations were shuffled and presented to the subject. The subject was required to select the vibration that most closely resembled the vibration generated from the five options, each of the five categories. This process was only conducted once to maintain an equal task number with the control group. We asked subjects to describe the vibration features and compare with the control group.

3. Select the corresponding target vibration for the vibration generated. The third part aimed to validate if subjects can identify differences between samples from a same class. The 45 shuffled generated vibrations were shown to the subjects. However, the references were changed to three vibrations in the same corresponding class. The subject needed to select the correct target vibration corresponding to the given generated vibration. The total number of classification tasks in this part was also 45.

Twenty subjects (11 males, 9 females, aged 22-27) took part in this stage. The entire process of the evaluation experiment lasted about 1.5 hours, including the tutorial and rest breaks.

Approval of all ethical and experimental procedures and protocols was granted by the Ethics Committee of The University of Tokyo.

## V. RESULTS

In this section we will first present the performance of the trained neural network model, and then present the results of the 2-stage user experiments.

#### A. Encoded Latent Space

The latent space is shown in Fig. 7 after the 50-epoch training process. With the benefit of the auxiliary classification, the latent space can be distinguished according to the class.



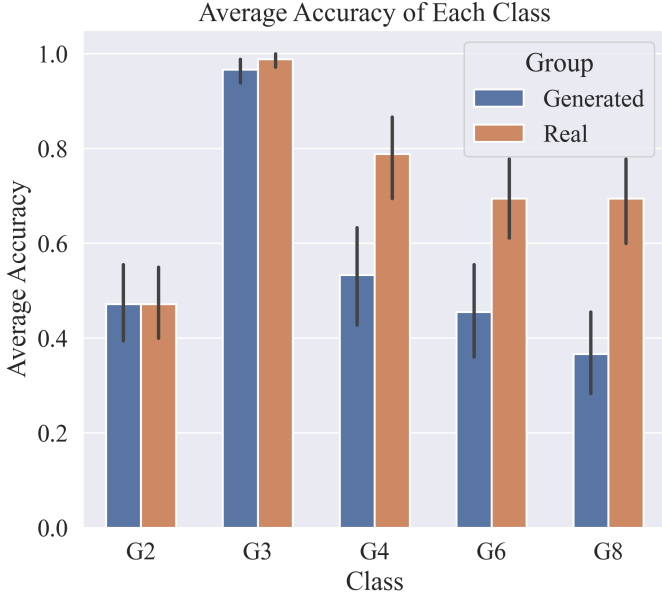


Fig. 9. The average accuracy was calculated in each class.

### B. Problems in Other Alternatives

In addition to the network model used in TEXasGAN, we implemented various other generators or decoders for comparison, including basic GAN, autoencoder; Variational Autoencoder (VAE) to learn the distribution; AAE to align the distribution, Conditional GAN (CGAN), and ACGAN to incorporate conditional information. However, these models faced challenges operating within our optimization framework, making direct comparisons unfeasible here.

At first we experimented with models based on the autoencoder architecture, namely autoencoder, VAE, and AAE. These models were easy to train but suffered from severe over-smoothing issues. As we needed feature vectors suitable for optimization, we aimed for a relatively small feature space dimension, such as the 128 dimensions used in this study. However, 128 proved insufficient for the original data, resulting in significant information loss when encoded into this latent space. Consequently, the generated spectrograms lacked detailed information, leading to substantial differences between the reconstructed vibrations and the original ones.

We also implemented GAN within our framework; however, it tended to suffer from mode collapse. Although it could generate spectrograms with more details compared to autoencoders, the model exhibited a strong tendency to produce similar results for different input. This behavior rendered it unsuitable for our optimization based on input vectors. In addition, GAN gives results from random noise generation, which brings about a mixed latent space. Therefore, as mentioned earlier in Sec. III-C and Sec. IV-C, the generated vibrations underwent drastic changes when the user continuously moved the slider. Unlike the original DSS research, which originally focused on visual stimuli, we emphasize tactile tasks, which have a much lower sensitivity compared to visual stimuli. Therefore, the abrupt changes pose difficulties for users in touching and comparing vibrations, making it nearly impossi-

ble for users to select an appropriate slider position.

We also compared generative models, CGAN and ACGAN, with conditional information support. Under our training framework, CGAN tended to produce extremely sparse output results or exhibited a tendency not to converge. ACGAN performed relatively better among the control group models we experimented with; however, it faced challenges when applied in the optimization process such as DSS. ACGAN can differentiate features between different classes and control them, but the uneven input vector format of label + latent vector is not conducive to the optimization process of DSS.

These problems make it difficult to identify models with similar performance for comparison with our TEXasGAN. Therefore, we have not provided the performance results or user studies of the control group in this regard.

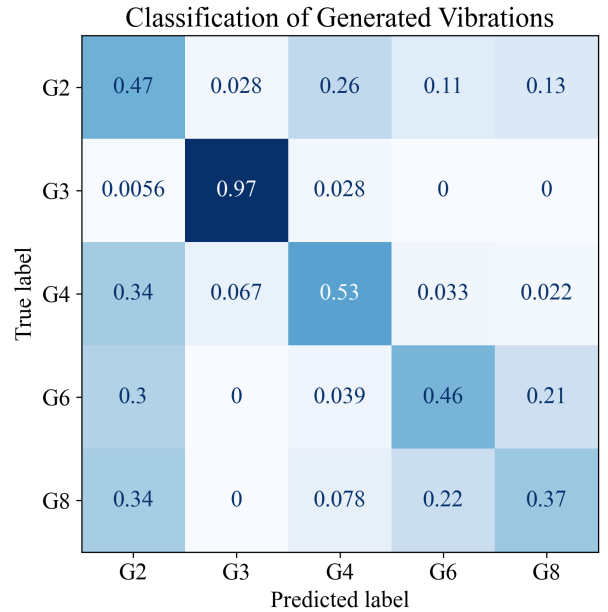


Fig. 10. The confusion matrix of the classification task of generated vibrations.

### C. User Study

Some generated samples of Stage I are shown in Fig. 8 to show the generation performance.

In the figure, the leftmost column shows five categories of target vibrations, while the three columns on the right show the vibrations generated by three users for these targets. We selected one vibration from each category for demonstration. The spectrograms reveal that our TEXasGAN successfully produces vibration patterns similar to the target for certain categories to a certain extent. While some results are less ideal, the tendency to generate more uniform vibration patterns shows the consistency of the system. This consistency is a strength, although it can make replicating vibrations with significant temporal fluctuations, like Grass Fiber, more challenging. Moreover, the GAN structure greatly aids in generation, but some detail loss brought by the autoencoder-like structure still results in smoother outputs compared to real

Classification of Real Vibrations

True label \ Predicted label	G2	G3	G4	G6	G8
G2	0.47	0.011	0.24	0.078	0.19
G3	0.0056	0.99	0.0056	0	0
G4	0.18	0.0056	0.79	0.011	0.017
G6	0.083	0	0.039	0.69	0.18
G8	0.094	0	0.044	0.17	0.69

Fig. 11. The confusion matrix of the classification task of real vibrations.

vibrations. Despite this, the system effectively replicates the general vibration characteristics to a certain extent, even if the intensity is slightly reduced compared to the original samples, such as Rough Paper.

However, spectrograms alone cannot fully capture the subjective experiences of the subjects. Therefore, we mainly focus on analyzing the results of Stage II, the classification task. From Fig. 9 we can see an overview of the result of the classification task. In the five-category task, subjects achieved an accuracy of 55.9% when judging the generated vibrations, compared to about 72.8% for the real vibrations. The control group results indicate that subjects can distinguish between different surface vibration stimuli. Fig. 9 shows that subjects in the generation group and the control group exhibited similar accuracy trends for these 5 kinds of different vibrations. This preliminary evidence suggests that our TEXasGAN can generate distinct vibration patterns that subjects can differentiate.

Fig. 10 shows the confusion matrix of the classification task of generated vibrations and Fig. 11 shows the control group, the classification of real vibrations. The confusion matrices provide a clearer view of how subjects distinguished between each type of vibration. We can see that both 2 confusion matrices show a diagonal trend.

The best generation was achieved with G3 vibrations, with a classification accuracy of 97% in the experimental group. The spectrogram shows that G3 has a higher proportion of high-frequency components compared to other categories. Subjects generally described G3 as a uniform and subtle high-frequency vibration. This distinct vibration pattern made it easier for subjects in Stage I to optimize the generated vibrations and for subjects in Stage II to distinguish this type of vibration.

Observing the confusion matrices, we find that their trends are similar but there are also some differences in accuracy

appearing in categories G4 (26%), G6 (23%) and G8 (32%). In the experimental group, subjects classified the generated G4 samples with an accuracy of 53%, G6 samples with an accuracy of 46% and G8 samples with an accuracy of 37%, while in the control group, the accuracy for G6 and G8 was 79%, 69% and 69%, respectively. Actually, we can find that the reason is that more G4, G6, and G8 samples were classified as G2. According to subject feedback, the characteristics of G2 vibrations are less distinct compared to other categories. Subjects often described G2 as a uniform and smooth mid-low frequency vibration or found it difficult to describe any prominent patterns. We can also notice that even in the control group, distinguishing the real G2 vibrations was challenging, with an accuracy of 47%, same as the generated group.

Additionally, we can draw some conclusions based on each subject's performance in both the generated and control group, as shown in Fig. 12. We calculated the average accuracy of each subject for each class, obtained 100 sets of accuracy. The figure roughly shows an interesting trend: subjects who were good at distinguishing real vibrations in the control group also tended to have higher classification accuracy in the generated group. To further illustrate this phenomenon, we constructed a multivariate regression model following the process below to verify the relationship between the accuracy in the control group and the accuracy in the generated group.

We constructed a linear regression model with interaction terms, using control group accuracy, subject ID, and vibration class as independent variables, and the generated group accuracy as the response. The model can be expressed as:

$$acc_G \sim 1 + c * i + c * acc_R + i * acc_R. \quad (6)$$

In the equation,  $acc_G$  represents the generated group accuracy,  $c$  represents the class,  $i$  represents the subject ID and  $acc_R$  represents the control group accuracy. Before the fit process, we removed outliers that were more than two scaled median absolute deviations from the median, obtained 93 sets of accuracy. Then we performed a stepwise regression to select significant variables. In this way, we can obtain a model like:

$$acc_G \sim 1 + c * acc_R. \quad (7)$$

This model keeps category  $c$  ( $p = 0.0699$ ), control group accuracy  $acc_R$  ( $p = 1.1785 \times 10^{-8}$ ), and their interaction term  $c * acc_R$  ( $p = 0.0012$ ). This shows that there is indeed a certain relationship between  $acc_R$  and  $acc_G$ . At the same time, the subject  $i$  ( $p = 0.4739$ ) is not a significant variable, indicating that this is a relatively common rule among subjects. The model  $R^2 = 0.423$ , means there is some certain relationship;  $F = 21.7$  with  $p = 1.19 \times 10^{-10}$ , means that the model is credited.

Furthermore, we can also obtain some information from the classification in a class. The overall 3-class classification accuracy is 42.2%. This in-class accuracy of each class is shown in Fig. 13. The accuracy of each class is 45.6% (G2), 46.1% (G3), 41.1% (G4), 36.1% (G6) and 42.2% (G8). Although the accuracy for each class is higher than the random classification for three classes (33.3%), indicating that there are indeed some differences between samples generated

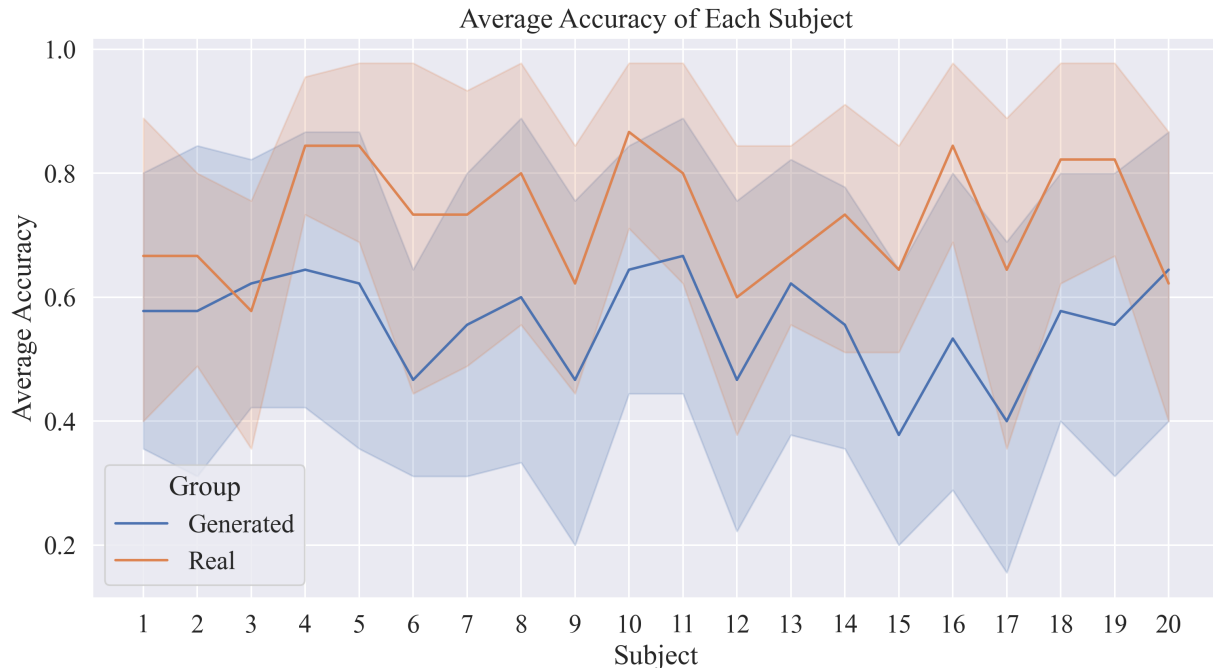


Fig. 12. The average accuracy of each subject.

with different targets, the classification accuracy is not high enough to prove that users can distinguish between samples belonging to the same class. This can be caused by the performance limitation of the model on the reconstruction of detailed information or the limited haptic resolution. However, in another aspect, this result suggests that the model captures and replicates some essential and general characteristics that define each class. Despite challenges in distinguishing within a class, participants were able to distinguish between different classes. This suggests that the system reliably encodes and reproduces the defining features of each kind of vibration.

## VI. DISCUSSION

From the results, we also observed several key phenomena that merit further discussion and analysis.

First, we can do some further discussion based on subjects' feedback and the patterns of these types of vibrations. The main frequency component of G4 vibrations is similar to G3 while the amplitude is stronger, similar to G2. Although the accuracy of real G4 achieves a high level, many subjects said G4 is difficult to distinguish comparing to G2. Just some subjects paying attention to frequencies can point out that G4 is "smooth", like G3 but less than G3. This observation helps explain why G2 and G4 are challenging to differentiate in the generated group.

This also suggests that subjects tend to use the intensity of the vibrations as their primary or initial criterion for the judgment. G6 vibrations are primarily composed of low-frequency components with uneven, strong, sudden pulses. And G8 vibrations are composed of some different frequency components, also strong but not so uneven as G6. Subjects who can pay attention to the frequency component can easily point out the differences but a lot of subjects just judge from the

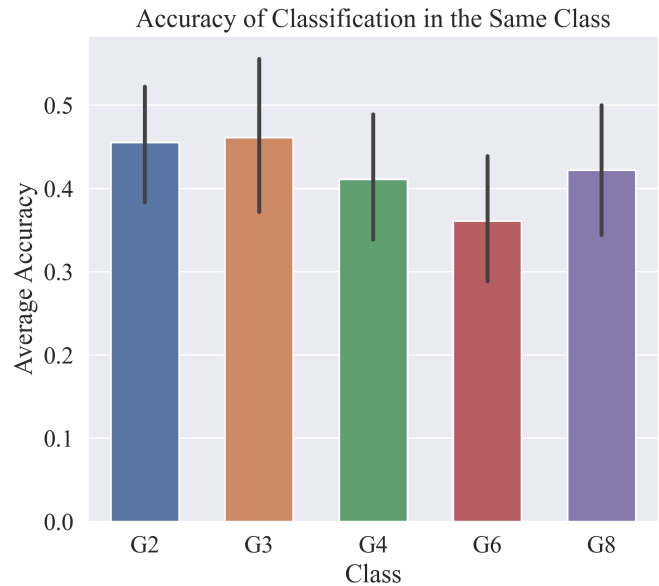


Fig. 13. The in-class accuracy of each class.

intensity and say they are similar. This phenomenon appears in both groups. Observing the spectrograms generated by users in Fig. 8 we notice that the model tends to produce uniform vibration patterns, making the generated vibrations similar to both G2 and G8. This similarity leads to confusion during classification as well.

Additionally, although the model incorporates GAN to mitigate detail loss due to feature space compression, some distortion is inevitable. As a result, the generated vibrations can exhibit an "oversmoothing" effect similar to that seen in

autoencoders, making them less “sharp” compared to the real vibrations. This can also reduce the uneven pulses present in the vibrations. For the same reasons, the intensity of the originally strong and rough surface, G8, is weakened. This makes it more similar to the more uniform and weaker G2. This aligns with subject feedback and the observation mentioned earlier that subjects tend to prioritize amplitude when making initial judgments.

Our demonstrated model can generate tactile vibrations that are distinguishable and aligned with target characteristics according to the user’s preference. However, there is still an obvious gap between the classification task accuracy of real samples and generated samples. Although there are some differences between the vibration feedback and textures, vibrations can activate some related receptors and give some similar perceptions [6]. Therefore, some related conclusions about texture perceptions may also explain phenomena in this research. A previous study points out that, eliminating movement constricted the subjective range of texture roughness or other surface features [32]. Because the haptic vibrations presented in this study are time-related rather than space-related, the participants did not experience spatial movement during their perception process. However, vibrational and spatial stimulation is considered 2 components of texture perception [33]. The accuracy of classification task may be influenced by this kind of stimulation absence, especially in experiment 3 of the Stage II which focuses on the detailed differences in the same class.

Additionally, the phenomenon in which users can distinguish between different classes but struggle to differentiate samples within the same class might be due to the model capturing more general information while having difficulty in capturing more specific information. This may be another kind of mode collapse. The mode collapse can occur in one of two forms: the intra-class mode collapse and the inter-class mode collapse [34]. Although we have incorporated conditional information to enable the model to generate samples across multiple categories and to control the generation process, thereby avoiding inter-category mode collapse, intra-category mode collapse can still occur. This can lead to the condition occurring in Stage I, where subjects, while exploring similar feature spaces, encounter the model’s tendency to produce similar results for a specific class or neighboring features. Consequently, this results in the model’s inability to capture specific details accurately, leading to a lower distinction accuracy among subjects in experiment 3, Stage II.

Therefore, in future work, we plan to explore other generative models to enhance the diversity and precision of the generated vibrations. For example, incorporating diffusion models could help improve the variety and fidelity of the output [35]. Diffusion models can be super easily to train compared with GAN and can provide high quality results. Additionally, the current optimization process is quite time consuming and requires subjects to focus intensely on detecting subtle differences while adjusting the slider position. Streamlining the interface for more intuitive operation could significantly improve user experience. To further create realistic interaction experiences, we will consider using devices that better simu-

late texture perception, integrating both spatial and temporal stimulation.

## VII. CONCLUSION

In conclusion, our study demonstrates the feasibility and effectiveness of a human-in-the-loop vibration generation system, TEXasGAN, to create realistic and distinguishable haptic textures. In our TEXasGAN model, we incorporate the idea of SRGAN and CAAE to generate class-controllable haptic vibrations with conditional information and encoded features. Using DSS and the pre-trained generative model, we enable users to intuitively control high-dimensional latent space and generate vibration samples using simple, one-dimensional sliders. The user experiments conducted with this system indicate that it can produce vibration patterns that are generally recognizable and distinguishable by subjects, though challenges remain in capturing finer, specific characteristics within specific classes. Overall, our approach offers a novel method for generating haptic vibrations based on user preferences, providing a foundation for future advancements in the field of haptic technology and virtual reality interactions.

## REFERENCES

- [1] Y. Monnai, K. Hasegawa, M. Fujiwara, K. Yoshino, S. Inoue, and H. Shinoda, “Haptomime: Mid-air haptic interaction with a floating virtual screen,” in *Proceedings of the 27th Annual ACM Symposium on User Interface Software and Technology*, ser. UIST ’14. New York, NY, USA: Association for Computing Machinery, 2014, p. 663–667. [Online]. Available: <https://doi.org/10.1145/2642918.2647407>
- [2] Q. Tong, W. Wei, Y. Zhang, J. Xiao, and D. Wang, “Survey on hand-based haptic interaction for virtual reality,” *IEEE Transactions on Haptics*, 2023.
- [3] D. Beattie, W. Frier, O. Georgiou, B. Long, and D. Ablart, “Incorporating the perception of visual roughness into the design of mid-air haptic textures,” in *ACM Symposium on Applied Perception 2020*, ser. SAP ’20. New York, NY, USA: Association for Computing Machinery, 2020. [Online]. Available: <https://doi.org/10.1145/3385955.3407927>
- [4] S. Cai, L. Zhao, Y. Ban, T. Narumi, Y. Liu, and K. Zhu, “GAN-based image-to-friction generation for tactile simulation of fabric material,” *Computers & Graphics*, vol. 102, pp. 460–473, 2022. [Online]. Available: <https://www.sciencedirect.com/science/article/pii/S009784932100193X>
- [5] T. Morisaki, M. Fujiwara, Y. Makino, and H. Shinoda, “Midair haptic-optic display with multi-tactile texture based on presenting vibration and pressure sensation by ultrasound,” in *SIGGRAPH Asia 2021 Emerging Technologies*, ser. SA ’21. New York, NY, USA: Association for Computing Machinery, 2021. [Online]. Available: <https://doi.org/10.1145/3476122.3484849>
- [6] M. Konyo, S. Tadokoro, A. Yoshida, and N. Saiwaki, “A tactile synthesis method using multiple frequency vibrations for representing virtual touch,” in *2005 IEEE/RSJ International Conference on Intelligent Robots and Systems*. IEEE, 2005, pp. 3965–3971.
- [7] S. Lu, M. Zheng, M. C. Fontaine, S. Nikolaidis, and H. Culbertson, “Preference-driven texture modeling through interactive generation and search,” *IEEE Transactions on Haptics*, vol. 15, no. 3, pp. 508–520, 2022.
- [8] Y. Koyama, I. Sato, D. Sakamoto, and T. Igarashi, “Sequential line search for efficient visual design optimization by crowds,” *ACM Trans. Graph.*, vol. 36, no. 4, jul 2017. [Online]. Available: <https://doi.org/10.1145/3072959.3073598>
- [9] C.-H. Chiu, Y. Koyama, Y.-C. Lai, T. Igarashi, and Y. Yue, “Human-in-the-loop differential subspace search in high-dimensional latent space,” *ACM Trans. Graph.*, vol. 39, no. 4, aug 2020. [Online]. Available: <https://doi.org/10.1145/3386569.3392409>
- [10] B. Sadia, S. E. Emgin, T. M. Sezgin, and C. Basdogan, “Data-driven vibrotactile rendering of digital buttons on touchscreens,” *International Journal of Human-Computer Studies*, vol. 135, p. 102363, 2020.

- [11] H.-R. Tsai, C. Tsai, Y.-S. Liao, Y.-T. Chiang, and Z.-Y. Zhang, "Fingerx: Rendering haptic shapes of virtual objects augmented by real objects using extendable and withdrawable supports on fingers," in *Proceedings of the 2022 CHI Conference on Human Factors in Computing Systems*, 2022, pp. 1–14.
- [12] Y. Toide, M. Fujiwara, Y. Makino, and H. Shinoda, "Sufficient time-frequency resolution for reproducing vibrotactile sensation," *IEEE Transactions on Haptics*, vol. 16, no. 3, pp. 412–423, 2023.
- [13] R. Hassen, B. Gülecüyüz, and E. Steinbach, "Pvc-slp: Perceptual vibrotactile-signal compression based-on sparse linear prediction," *IEEE Transactions on Multimedia*, vol. 23, pp. 4455–4468, 2021.
- [14] A. Noll, L. Nockenberger, B. Gülecüyüz, and E. Steinbach, "Vc-pwq: Vibrotactile signal compression based on perceptual wavelet quantization," in *2021 IEEE World Haptics Conference (WHC)*. IEEE, 2021, pp. 427–432.
- [15] A. Noll, M. Hofbauer, E. Muschter, S.-C. Li, and E. Steinbach, "Automated quality assessment for compressed vibrotactile signals using multi-method assessment fusion," in *2022 IEEE Haptics Symposium (HAPTICS)*. IEEE, 2022, pp. 1–6.
- [16] G. Liu, X. Li, C. Wang, and S. Lv, "Online compression and reconstruction for communication of force-tactile signals," *IEEE Communications Letters*, vol. 27, no. 3, pp. 981–985, 2023.
- [17] Z. Li, R. Hassen, and Z. Wang, "Autoencoder for vibrotactile signal compression," in *ICASSP 2021-2021 IEEE International Conference on Acoustics, Speech and Signal Processing (ICASSP)*. IEEE, 2021, pp. 4290–4294.
- [18] Y. Ban and Y. Ujitoko, "Tactgan: Vibrotactile designing driven by gan-based automatic generation," in *SIGGRAPH Asia 2018 Emerging Technologies*, ser. SA '18. New York, NY, USA: Association for Computing Machinery, 2018. [Online]. Available: <https://doi-org.utokyo.idm.oclc.org/10.1145/3275476.3275484>
- [19] S. Cai, K. Zhu, Y. Ban, and T. Narumi, "Visual-tactile cross-modal data generation using residue-fusion gan with feature-matching and perceptual losses," *IEEE Robotics and Automation Letters*, vol. 6, no. 4, pp. 7525–7532, 2021.
- [20] Y. Fang, Y. Qiao, F. Zeng, K. Zhang, and T. Zhao, "A human-in-the-loop haptic interaction with subjective evaluation," *Frontiers in Virtual Reality*, vol. 3, p. 949324, 2022.
- [21] L. Chan, Y.-C. Liao, G. B. Mo, J. J. Dudley, C.-L. Cheng, P. O. Kristensson, and A. Oulasvirta, "Investigating positive and negative qualities of human-in-the-loop optimization for designing interaction techniques," in *Proceedings of the 2022 CHI Conference on Human Factors in Computing Systems*, 2022, pp. 1–14.
- [22] C. Ledig, L. Theis, F. Huszár, J. Caballero, A. Cunningham, A. Acosta, A. Aitken, A. Tejani, J. Totz, Z. Wang *et al.*, "Photo-realistic single image super-resolution using a generative adversarial network," in *Proceedings of the IEEE conference on computer vision and pattern recognition*, 2017, pp. 4681–4690.
- [23] Y. Ujitoko and Y. Ban, "Vibrotactile signal generation from texture images or attributes using generative adversarial network," in *Haptics: Science, Technology, and Applications*, D. Prattichizzo, H. Shinoda, H. Z. Tan, E. Ruffaldi, and A. Frisoli, Eds. Cham: Springer International Publishing, 2018, pp. 25–36.
- [24] A. Odena, C. Olah, and J. Shlens, "Conditional image synthesis with auxiliary classifier gans," in *International conference on machine learning*. PMLR, 2017, pp. 2642–2651.
- [25] C. Lazarou, "Autoencoding generative adversarial networks," *arXiv preprint arXiv:2004.05472*, 2020.
- [26] Z. Zhang, Y. Song, and H. Qi, "Age progression/regression by conditional adversarial autoencoder," in *Proceedings of the IEEE conference on computer vision and pattern recognition*, 2017, pp. 5810–5818.
- [27] A. Makhzani, J. Shlens, N. Jaitly, I. Goodfellow, and B. Frey, "Adversarial autoencoders," *arXiv preprint arXiv:1511.05644*, 2015.
- [28] M. Strese, C. Schuwerk, A. Iepure, and E. Steinbach, "Multimodal feature-based surface material classification," *IEEE transactions on haptics*, vol. 10, no. 2, pp. 226–239, 2016.
- [29] D. Griffin and J. Lim, "Signal estimation from modified short-time fourier transform," *IEEE Transactions on acoustics, speech, and signal processing*, vol. 32, no. 2, pp. 236–243, 1984.
- [30] Y.-Y. Yang, M. Hira, Z. Ni, A. Chourdia, A. Astafurov, C. Chen, C.-F. Yeh, C. Puhrsch, D. Pollack, D. Genzel, D. Greenberg, E. Z. Yang, J. Lian, J. Mahadeokar, J. Hwang, J. Chen, P. Goldsborough, P. Roy, S. Narenthiran, S. Watanabe, S. Chintala, V. Quenneville-Bélair, and Y. Shi, "Torchaudio: Building blocks for audio and speech processing," *arXiv preprint arXiv:2110.15018*, 2021.
- [31] F. Glover, "Future paths for integer programming and links to artificial intelligence," *Computers & Operations Research*, vol. 13, no. 5, pp. 533–549, 1986, applications of Integer Programming.
- [32] M. Hollins and S. R. Risner, "Evidence for the duplex theory of tactile texture perception," *Perception & psychophysics*, vol. 62, no. 4, pp. 695–705, 2000.
- [33] D. Katz and L. E. Krueger, *The world of touch*. Psychology press, 2013.
- [34] M. M. Saad, M. H. Rehmani, and R. O'Reilly, "Addressing the intra-class mode collapse problem using adaptive input image normalization in gan-based x-ray images," in *2022 44th annual international conference of the IEEE Engineering in Medicine & Biology Society (EMBC)*. IEEE, 2022, pp. 2049–2052.
- [35] J. Ho, A. Jain, and P. Abbeel, "Denoising diffusion probabilistic models," *Advances in neural information processing systems*, vol. 33, pp. 6840–6851, 2020.